Structural and Multidisciplinary Optimization manuscript No.
(will be inserted by the editor)

Robert Lipton · Michael Stuebner

Optimal design of composite structures for strength and stiffness: an inverse homogenization approach

Preprint: To Appear in Structural and Multidisciplinary Optimization 2007

Abstract We introduce a rigorously based numerical method for compliance minimization problems in the presence of point wise stress constraints. The method is based on new multiscale quantities that measure the amplification of the local stress due to the microstructure. The design method is illustrated for two different kinds of problems. The first identifies suitably graded distributions of fibers inside shaft cross sections that impart sufficient overall stiffness while at the same time adequately control the amplitude of the local stress at each point. The second set of problems are carried out in the context of plane strain. Here we recover a novel class of designs made from locally layered media for minimum compliance subject to point wise stress constraints. The stress constrained designs place the more compliant material in the neighborhood of stress concentrators associated with abrupt changes in boundary loading and reentrant corners.

Keywords Stress constraints · Optimal structural design

This research is supported by NSF through grant DMS-0406374 and by the Air Force Office of Scientific Research, Air Force Materiel Command USAF, under grant numbers F49620-02-1-0041 and FA9550-05-1-0008.

R. Lipton
Department of Mathematics
Louisiana State University
Baton Rouge, LA 70803 Tel.: +1-225-5781569
Fax: +1-225-5784276
E-mail: lipton@math.lsu.edu

M. Stuebner
Department of Mathematics
Louisiana State University
Baton Rouge, LA 70803
Tel.: +1-225-5787989
Fax: +1-225-5784276
E-mail: stuebner@math.lsu.edu

1 Introduction

It is now well established that homogenization theory is an effective tool for the design of composites for optimal structural compliance and natural frequency see Allaire (2002), Bendsøe and Sigmund (2003), Cherkaev and Kohn (1997), Cherkaev (2000), Lewinski and Telega (2000), Lurie (1993), Olhoff (1996), Tartar (2000). On the other hand relatively little work has been directed towards the solution of stress constrained composite design problems. Recently new efforts have initiated the development of numerical methods for structural optimization in the presence of stress constraints. The investigation given in Duysinx and Bendsøe (1998) provides a numerical method for the stress constrained minimum volume design problem. The method is carried out using an empirical model known as the Solid Isotropic Microstructure with Penalization (SIMP) model, see Bendsøe and Sigmund (2003). The problem of mean square stress constrained structural optimization for fiber reinforced shafts is taken up in Lipton (2002). In that work a numerical algorithm is developed based on a suitable homogenized quantity (the covariance tensor) that rigorously encodes the mean square stress constraints. The work of Allaire, Jouve and Mallot (2004) introduces a partial relaxation for topology optimization for minimum mean square stress using finite rank laminates.

The general theory behind the homogenization approach to mean square stress (or gradient) constrained structural optimization is significantly different from the theory of compliance minimization. It is demonstrated in Lipton (2002), Lipton (2004) that the associated relaxed problem formulation requires the use of the derivatives of G-limits in addition to using the theory of effective properties (G-limits). Alternative theoretical treatments for the related scalar problem of minimizing the mean square distance of the gradient from a target have been developed in the earlier work of Tartar (1994) and subsequent work presented in Velo (2000), Grabovsky (2001), Lipton and Velo (2002), Pedregal (2004) and Donso and Pedre-

gal (2005). These methods can naturally be rephrased in terms of G-limits and their derivatives. All of these methods invoke the use of suitable homogenized or multiscale quantities for the design of local microgeometry. For this reason these approaches may be considered inverse homogenization methods.

In this paper we present a new rigorously based numerical approach to the problem of microstructure design for minimum compliance subject to pointwise stress constraints. Here the objective is to design a graded microstructure in order to control local stress in the vicinity of stress concentrations. The methodology used here has been developed by the authors in Lipton (2004), Lipton and Stuebner (2006a), Lipton and Stuebner (2006b) and is based upon new rigorous multiscale stress criteria that connect the macroscopic or homogenized stress to the local stress at the scale of the microstructure, see Lipton (2003), Lipton (2004). The multiscale criteria are given in terms of quantities dubbed macro stress modulation functions. Here we show how to apply these multiscale quantities to develop an inverse homogenization approach for minimum compliance design subject to point wise stress constraints. The homogenized design formulation considered here is expressed in terms of homogenized stress and strain fields and macro stress modulation functions. The homogenized design problem satisfies two requirements: The first is that the homogenized design problem is computationally
tractable. The second is that the solution of the homogenized design problem provides the means to identify graded microstructures that deliver the required structural response while at the same time provide control on the point wise values of the stress inside the composite.

The design method is illustrated for two different kinds of problems. The first type of problem is to identify suitably graded distributions of fibers inside shaft cross sections that impart sufficient overall stiffness while at the same time adequately control the intensity of the local stress. This problem is solved numerically in Section 3. The second set of examples are carried out in the context of plane strain. In these examples we consider designs made from locally layered media. Here we exhibit novel minimum compliance designs that are subject to point wise stress constraints, see Section 4. These designs are shown to drastically reduce the point wise stress below the stress levels seen in the minimum compliance designs. The new stress constrained designs feature zones of compliant material surrounding stress concentrators due to abrupt changes in boundary loading and reentrant corners.

This paper touches on several topics that have been part of the work of Pauli Pedersen, these include material optimization, shape design, and stress constraints. The authors would like to dedicate this article to Professor Pedersen on the occasion of his 70^{th} birthday.

2 Homogenized design formulation and identification of optimally graded fiber reinforced shafts.

We start by illustrating our approach for the first design problem. Here we consider fiber reinforcement of a long shaft with constant cross section subjected to torsion loading, see Love (1944). The microstructure within the shaft consists of long reinforcement fibers of constant cross section with isotropic shear modulus G_f embedded in a more compliant material with shear modulus G_m. The shaft together with the fibers are right cylinders with generators along the x_3 axis. The cross section of the reinforced shaft is specified by a fixed region Ω in the $x_1 - x_2$ plane. The shaft cross section is divided up into many square cells. Each cell contains a single fiber cross section. The fiber cross section is circular and is centered inside the square cell. The radii of the fiber inside each cell is chosen independently of the others. The characteristic length scale of the square cells relative to the size of the design domain is denoted by ε. Our design problem is carried out when the total fiber cross-sectional area is constrained to be 40% and for $\varepsilon = 0.1$. The goal of the design problem is to identify a graded distribution of fibers across the cross section such that the following requirements are met:

I. The reinforced shaft has a torsional rigidity that is acceptable.

II. The magnitude of the local point wise stress inside the composite is controlled over a designated subset of the cross section.

To illustrate the ideas we develop the inverse homogenization design method within the context of this problem. The inverse homogenization design method is a top down design approach. First a well posed homogenized design problem is developed. This design problem is given in terms of design variables that reflect the local microgeometry inside the composite. For the problem treated here the design variable for the homogenized design problem is given by the local density of fibers $\theta_f(\mathbf{x})$. The homogenized design problem is then solved to obtain an optimal density function $\hat{\theta}_f(\mathbf{x})$. With the optimal density in hand we use it to recover an explicit graded fiber design that has structural properties close to that of the optimal homogenized design and satisfies prescribed point wise stress constraints. Such a fiber design is shown in Figure 5. The subsections are organized as follows, we begin by describing the homogenized design problem and then provide the explicit link between homogenized designs and graded fiber reinforced designs that satisfy point wise stress constraints.

2.1 Homogenized design problem

The design variable for the homogenized design problem is given by the density function $\theta_f(\mathbf{x})$. This function is interpreted as providing the local area fraction of the fiber phase in a homogenized design. The resource constraint on the fiber phase is given by

$$\int_{\Omega} \theta_f(\mathbf{x})\, dx_1 dx_2 \leq \Theta \times (Area\ of\ \Omega), \tag{2.1}$$

where $0 < \Theta < 1$. At each point the local area fraction satisfies the box constraint given by

$$0 < \theta_f^{min} \leq \theta_f \leq \theta_f^{max} < 1. \tag{2.2}$$

Here the upper and lower bounds given in (2.2) correspond to the entire design domain being filled with composite material. In this treatment the local fiber area fraction θ_f changes continuously with position according to the condition

$$|\theta_f(\mathbf{x}) - \theta_f(\mathbf{x}+\mathbf{h})| \leq K|\mathbf{h}|. \tag{2.3}$$

Here the constant K is prescribed by the designer. The universe of admissible designs given by all local area fractions θ_f satisfying the resource constraint, box constraints, and (2.3) is denoted by D_Θ.

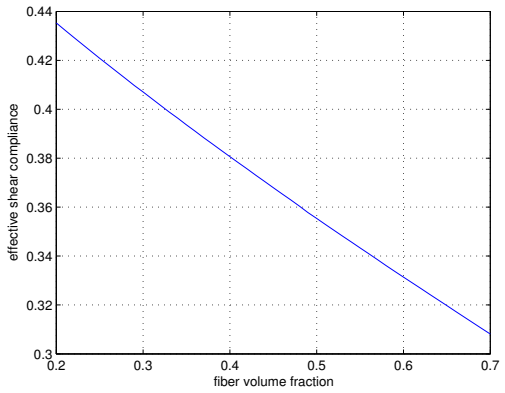

Fig. 1 Plot of s^E.

The compliance in shear for the matrix and fiber are given by $S_m = (2G_m)^{-1}$ and $S_f = (2G_f)^{-1}$ respectively. Here the matrix is more compliant and $S_m > S_f$. For a given $\theta_f(\mathbf{x})$ we introduce the effective shear compliance $S^E(\theta_f(\mathbf{x}))$ associated with a locally periodic microgeometry made from fibers with circular cross sections centered inside square unit cells. The unit period cell for this configuration is denoted by Q. The area fraction of Q occupied by the fiber cross section is set to $\theta_f(\mathbf{x})$. The shear compliance inside Q is written $S(\theta_f(\mathbf{x}), \mathbf{y})$ and takes the value S_f for points $\mathbf{y}$ in the fiber and S_m for $\mathbf{y}$ in the matrix. The unit vectors $\mathbf{e}^1 = (1,0)$ and $\mathbf{e}^2 = (0,1)$ are introduced and for each $\mathbf{x}$ in Ω we introduce the periodic

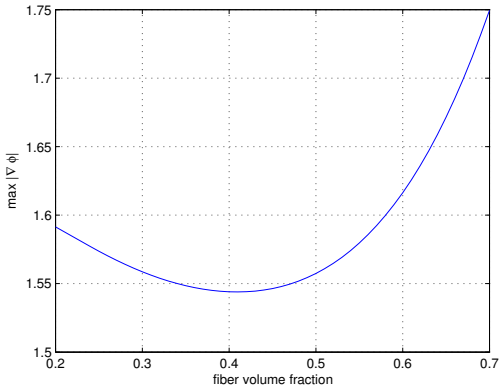

Fig. 2 Plot of $A(\theta_f)$.

fluctuating stress potentials $w^i(\mathbf{x}, \mathbf{y})$, $i = 1, 2$ that solve the microscopic equilibrium equation

$$-\text{div}_{\mathbf{y}}\left(S(\theta_f(\mathbf{x}), \mathbf{y})(\nabla_{\mathbf{y}} w^i(\mathbf{x}, \mathbf{y}) + \mathbf{e}^i)\right) = 0 \tag{2.4}$$

for $\mathbf{y}$ in Q. Here the $\mathbf{x}$ coordinate appears a parameter and all differentiations are carried out with respect to the $\mathbf{y}$ variable. The effective compliance tensor is a function of the local area fraction of fibers θ_f and from symmetry the effective compliance tensor is isotropic and given by

$$[S^E(\theta_f(\mathbf{x}))]_{ij} = s^E(\theta_f(\mathbf{x}))\delta_{ij} \tag{2.5}$$

where the effective compliance is given by

$$s^E(\theta_f(\mathbf{x})) = \left(\int_Q S(\theta_f(\mathbf{x}), \mathbf{y})(\partial_{y_1} w^1(\mathbf{x}, \mathbf{y}) + \mathbf{e}_1^1)\, d\mathbf{y}\right). \tag{2.6}$$

A graph of s^E plotted as a function of θ_f is given in Figure 1 for the choice $S_m = 0.5$ and $S_f = 0.25$.

The macroscopic stress potential ϕ^H vanishes on the boundary of the shaft cross section and satisfies

$$-\text{div}\left(S^E(\theta_f)\nabla\phi^H\right) = 1 \tag{2.7}$$

inside the cross section. The torsional rigidity for the homogenized shaft cross section made from a homogenized material with compliance $S^E(\theta_f)$ is given by

$$\mathcal{R}(\theta_f) = 2\int_{\Omega} \phi^H\, dx_1 dx_2. \tag{2.8}$$

The macroscopic stress in the homogenized shaft is given by $\sigma^H = R\nabla\phi^H$ where R is the rotation matrix associated with a counter clockwise rotation of $\pi/2$ radians.

The multiscale stress criterion is given in terms of the macro stress modulation function introduced in Lipton (2003). The macro stress modulation function captures the interaction between the macroscopic stress $\sigma^H(\mathbf{x})$ and the microstructure. The microscopic response to the imposed macroscopic stress is given by

$$\sigma(\mathbf{x}, \mathbf{y}) = R[\sum_{i=1}^{2}(\nabla_{\mathbf{y}}(w^i(\mathbf{x}, \mathbf{y})) + \mathbf{e}^i)\partial_{x_i}\phi^H(\mathbf{x})].$$

The relevant interaction is described by the macro stress modulation function $f(\theta_f, \sigma^H)$ given by

$$f(\theta_f(\mathbf{x}), \sigma^H(\mathbf{x})) = \sup_{\mathbf{y} \text{ in } Q} \{|\sigma(\mathbf{x}, \mathbf{y})|\}. \tag{2.9}$$

Physically the macro stress modulation provides an upper envelope on the oscillating point wise local stress in the composite, see Lipton (2003).

From the symmetry of the microstructure it easily follows that macro stress modulation for a locally periodic microgeometry made from fibers with circular cross sections centered inside square unit cells is of the form

$$f(\theta_f(\mathbf{x}), \sigma^H(\mathbf{x})) = A(\theta_f(\mathbf{x}))|\nabla\phi^H(\mathbf{x})|, \tag{2.10}$$

where for $0 < \theta_f^{min} \leq \theta_f \leq \theta_f^{max} < 1$,

$$A(\theta_f) = \sup_{\mathbf{y} \text{ in } Q} \{|\nabla_{\mathbf{y}} w^1(\mathbf{x}, \mathbf{y}) + \mathbf{e}^1|\}. \tag{2.11}$$

A graph of the local stress amplification factor $A(\theta_f)$ as function of θ_f is given in Figure 2 for the choice $S_m = 0.5$ and $S_f = 0.25$.

We enforce the stress constraint by adding a penalty term to the torsional rigidity and the homogenized design problem is to minimize

$$L(\theta_f) = -\mathcal{R}(\theta_f) + l \int_\Omega (f(\theta_f, \nabla\phi^H))^p \, dx_1 dx_2, \tag{2.12}$$

over all θ_f in D_Θ where $l > 0$ and ϕ^H satisfies

$$-\text{div}\left(S^E(\theta_f)\nabla\phi^H\right) = 1 \tag{2.13}$$

and vanishes at the boundary. The computational examples are carried out for a domain with reentrant corners of interior angle $3\pi/2$. In view of the strength of the associated singularity at the reentrant corners the power "p" appearing in the penalty term is chosen to be less than 3. We mention in closing that (2.3) provides a constraint on the spatial variation of the homogenized designs. This constraint provides the compactness necessary for a well posed design problem Lipton (2004). We point out that in our numerical simulations for the fiber reinforced shaft we have relaxed the constraint (2.3) and discretized θ_f using linear triangular elements.

2.2 Identification of graded fiber design from the homogenized design

In this subsection it is shown how to use the optimal design $\hat{\theta}_f$ for the homogenized problem to identify a graded fiber design satisfying the requirements (I) and (II). The examples considered in this treatment are given for a structural domain specified by an "X" shaped cross section. All interior angles for the reentrant corners are fixed at $3\pi/2$ radians. The tip to tip length of each leg of the "X" shaped domain is 2cm. The width of each leg is 2/3 cm. In order to describe the graded fiber composite, the shaft cross section Ω is partitioned into the N square subdomains $\mathcal{S}^k$, $k = 1, \ldots, N$ and $\Omega = \cup_k^N \mathcal{S}^k$. The side length of these subdomains is given by ε.

The building block for the microstructure is the square unit cell filled with a centered circular fiber cross section. The area fraction of the fiber phase inside the unit cell is given by θ_f. A microstructure is obtained by rescaling the unit cell by the factor $\varepsilon \times \nu$ so that it becomes the period cell for a $\varepsilon \times \nu$ periodic composite. A graded fiber composite is constructed by placing an $\varepsilon \times \nu$ periodic composite inside each square subdomain $\mathcal{S}^k$. The area fraction of fibers in each subdomain is given by the constant θ_f^k and these constants can change between subdomains. We note that choosing $\nu = 1$ corresponds to placing one fiber cross section inside $\mathcal{S}^k$. Higher values of ν correspond to progressively finer periodic distributions of fiber cross sections inside $\mathcal{S}^k$.

For future reference this type of locally periodic microstructure will be called a (ε, ν)-graded periodic fiber microstructure.

The local piecewise constant shear compliance for the (ε, ν)-graded periodic fiber microstructure is denoted by $S^{\varepsilon,\nu}$. The stress potential for this microstructure is denoted by $\phi^{\varepsilon,\nu}$ and vanishes on the boundary of the cross section. The stress potential satisfies the equilibrium equation

$$-\text{div}\ (S^{\varepsilon,\nu}\nabla\phi^{\varepsilon,\nu}) = 1. \tag{2.14}$$

The torsional rigidity of the cross section is given by

$$\mathcal{R}^{\varepsilon,\nu} = 2\int_\Omega \phi^{\varepsilon,\nu} \, dx_1 dx_2. \tag{2.15}$$

The nonzero components of the in plane stress are denoted by the vector $\sigma^{\varepsilon,\nu} = (\sigma_{13}^{\varepsilon,\nu}, \sigma_{23}^{\varepsilon,\nu})$ and are related to the gradient of the stress potential according to

$$\sigma^{\varepsilon,\nu} = R\nabla\phi^{\varepsilon,\nu}. \tag{2.16}$$

Here R is the matrix corresponding to a counter clockwise rotation of $\pi/2$ and $|\sigma^{\varepsilon,\nu}| = |\nabla\phi^{\varepsilon,\nu}|$.

The relation between the optimal design for the homogenized problem and the point wise stress and torsional rigidity for the (ε, ν)-graded periodic fiber microstructure is given in the following Theorem, see Lipton (2004) and Lipton and Stuebner (2006b).

Theorem 2.1. Identification of graded microstructure.
Given the minimizing density $\hat{\theta}_f$ and associated stress potential $\hat{\phi}^H$ for the homogenized problem we consider sets of the form

$$A_T = \{\mathbf{x} \in \Omega : \ f(\hat{\theta}_f(\mathbf{x}), \nabla\hat{\phi}^H(\mathbf{x})) \leq T\}. \tag{2.17}$$

For fixed choices of $\delta > 0$ and $t > T$ one can choose ε and ν small enough such that the (ε, ν)-graded periodic

microstructure for which the the part of A_T over which the stress constraint

$$|\nabla\phi^{\varepsilon,\nu}(\mathbf{x})| \leq t \tag{2.18}$$

is violated has measure (area) less than δ and

$$|\mathcal{R}^{\varepsilon,\nu} - \mathcal{R}(\hat{\theta}_f)| < \delta, \tag{2.19}$$

with

$$\sum_{k=1}^{\hat{N}} |\mathcal{S}^k| \hat{\theta}_f^k \leq \Theta \times (Area\, of\, \Omega) + \delta. \tag{2.20}$$

For these designs the area fractions of the fibers inside each $\mathcal{S}^k$ are denoted by $\hat{\theta}_f^k$ and are chosen according to

$$\hat{\theta}_f^k = \frac{1}{|\mathcal{S}^k|} \times \int_{\mathcal{S}^k} \hat{\theta}_f(\mathbf{x}) dx_1 dx_2. \tag{2.21}$$

The homogenized design formulation together with the identification Theorem comprise the inverse homogenization method for identifying microstructures that satisfy point wise stress constraints while delivering a torsional rigidity close to that given by the optimal design $\hat{\theta}_f$ for the homogenized design problem.

3 Inverse homogenization and graded fiber designs for the X-shaped cross section

In this section we demonstrate the methodology for fiber reinforced shafts. The calculations were carried out using the gradient minimization algorithm introduced in Lipton and Stuebner (2006b) and Lipton and Stuebner (2006a). All calculations are done for the choice $p = 1$ in the Lagrangian (2.12). The shear stiffness of the matrix is assigned the value $G_m = 1\, GPa$ and the shear stiffness of the fiber phase is assigned the value $G_f = 2\, GPa$. For these choices $S_m = 1/(2G_m) = 0.5$ and $S_f = 1/(2G_f) = 0.25$. For this example θ_f is constrained to lie between $0.2 \leq \theta_f \leq 0.7$ and $\int_\Omega \theta_f = 0.4 \times Area\, of\, \Omega$. A plot of the fiber density field $\hat{\theta}_f$ is given in Figure 3. The contour plots of the macro stress modulation function $f(\hat{\theta}_f(\mathbf{x}), \nabla\hat{\phi}^H(\mathbf{x}))$ is given in Figure 4.

The (ε, ν)-graded periodic microstructure is constructed from the optimal homogenized design according to the prescription of Theorem 2.1. Here we compute the average of $\hat{\theta}_f(\mathbf{x})$ over each square $\mathcal{S}^k$ according to (2.21) and denote it by $\hat{\theta}_f^k$. The area fraction of the fibers in $\mathcal{S}^k$ is set to $\hat{\theta}_f^k$. The design is computed for the choice $\varepsilon = 0.1$ and $\nu = 1$. The discrete fiber design is displayed in Figure 5.

The level lines of the magnitude of the stress field in the actual fiber reinforced design is plotted in Figure 6. It follows from Figures 4 and 6 that the point wise stress behavior is well represented by the level curves of the macro stress modulation function for the optimal homogenized design.

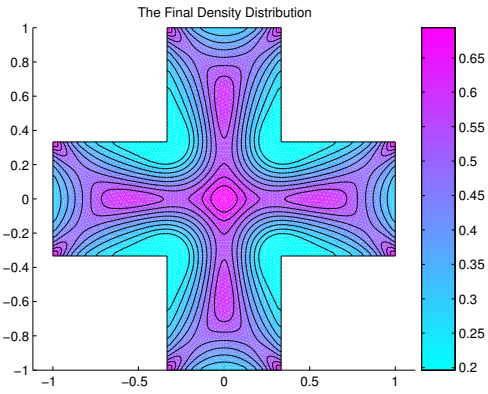

Fig. 3 Grey scale plot of the local area fraction of fibers $\hat{\theta}_f(\mathbf{x})$.

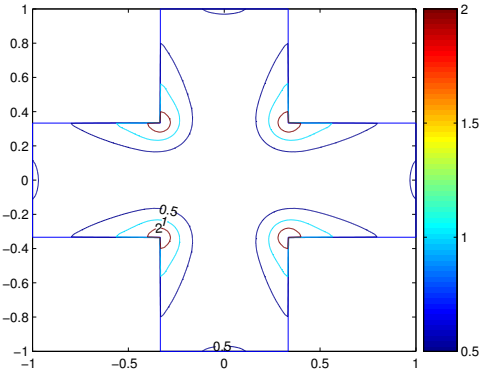

Fig. 4 Contour plot of $f(\hat{\theta}_f(\mathbf{x}), \nabla\phi^H(\mathbf{x}))$

4 Graded locally layered media and 2 dimensional elastic design

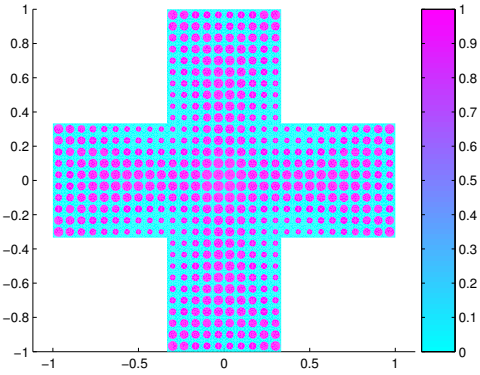

Fig. 5 Graded fiber design.

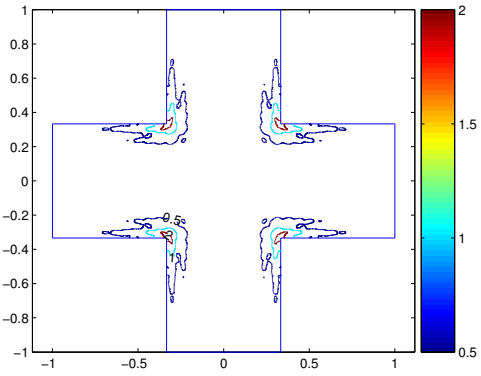

Fig. 6 Contour plot of the magnitude of the local stress amplitude.

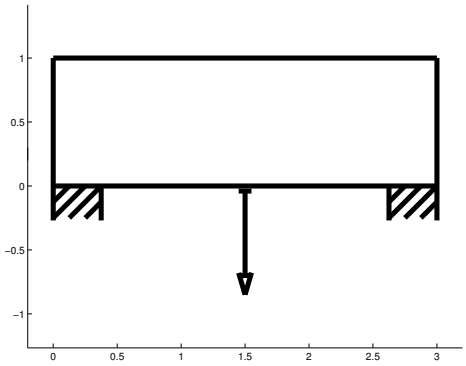

Fig. 7 Loading for the rectangular domain for the plane strain problem.

For our second set of examples we consider a long beam of fixed cross section and we suppose that the loading is the same for every cross section. This is the classic case of plain strain loading Love (1944). We first consider rectangular cross sections with loading and boundary conditions illustrated in Figure 7. For this case the microgeometry is made up of locally layered material made from two linearly elastic components. The layers consist of long rectangular fibers with constant cross section with generators parallel to the beam. The design variables are the relative thicknesses of the layers and their orientation and these can change across the rectangular cross section as indicated in Figure 8.

In this section we generate optimal locally layered designs for three distinct design criteria. The first is to design for minimum overall compliance, the second is to design for point wise stress minimization and the third is to design for minimum compliance subject to a penalty on the magnitude of the point wise stresses. The homogenization methodology for optimal compliance design requires one to use only the effective elastic properties of the layered elastic medium, see Bendsøe and Sigmund (2003). However in order to design for the second two criteria we will need to also use the macro stress modulation function associated with layered materials.

The two component materials are elastically isotropic and well ordered with Young's moduli $E_1 > E_2$ and equal Poisson's ratio $\nu_1 = \nu_2$. The effective elastic tensor for the layered material depends upon the relative local relative layer thickness of material one and the layer orientation. The local layer thickness of material one is denoted by θ_1. The layer orientation is specified by the local unit vector normal to the layers and is denoted by $\mathbf{n}$. The elastic tensor for each material is denoted by A_1 and A_2 and the formula for the effective elasticity is given by Francfort and Murat (1987)

$$A^L(\theta_1, \mathbf{n}) = A_1 + \theta_1 \left[(A_1 - A_2)^{-1} + (1-\theta_1)\Gamma(\mathbf{n})\right]^{-1}, \tag{4.1}$$

where $\Gamma(\mathbf{n})$ is given by

$$\Gamma(\mathbf{n})\eta : \eta = \frac{1}{\mu_1}(|\eta\mathbf{n}|^2 - (\eta\mathbf{n}\cdot\mathbf{n})^2) + \frac{1}{2\mu_1+\lambda_1}(\eta\mathbf{n}\cdot\mathbf{n})^2, \tag{4.2}$$

for any constant strain η. Here the shear modulus μ_1 and Lame coefficient λ_1 are those associated with plane strain. The homogenized stress σ^H is related to the homogenized strain e^H by

$$\sigma^H = A^L(\theta_1, \mathbf{n})e^H. \tag{4.3}$$

The elastic strain $e^H = 1/2(u^H_{i,j} + u^H_{j,i})$ is the symmetrized gradient of the elastic displacement $\mathbf{u}^H$. The elastic displacement is the solution of the equilibrium problem

$$\text{div}\left(A^L e^H\right) = 0, \tag{4.4}$$

and satisfies the displacement and traction conditions given in Figure 7. Following Stuebner (2006) the macro stress modulation function associated with material one for the layered material is given by

$$f_1(\theta_1, \sigma^H(\mathbf{x})) = |A_1\overline{\zeta}|^2, \tag{4.5}$$

where

$$\overline{\zeta} = A_1\overline{\eta} + \frac{(1-\theta_1)}{2}A_1(\mathbf{p}\otimes\mathbf{n} + \mathbf{n}\otimes\mathbf{p}) \tag{4.6}$$

and $\overline{\eta} = (A^L)^{-1}\sigma^H$. Here $\otimes$ denotes the tensor product of two vectors and

$$\mathbf{p} = \frac{\Delta\mu}{\langle\tilde{\mu}\rangle}(2\overline{\eta}\mathbf{n} - tr\{\overline{\eta}\}\mathbf{n}) + \frac{\Delta\kappa}{\langle\tilde{\mu}\rangle}tr\{\overline{\eta}\}\mathbf{n} - \frac{\langle\tilde{\kappa}\rangle}{\langle\tilde{\mu}\rangle}\left(\frac{\Delta\mu(2\overline{\eta}\mathbf{n}\cdot\mathbf{n} - tr\{\overline{\eta}\}) + \Delta\kappa tr\{\overline{\eta}\}}{\langle\tilde{\mu}\rangle + \langle\tilde{\kappa}\rangle}\right)\mathbf{n}, \tag{4.7}$$

where $\Delta\mu = \mu_2 - \mu_1$, $\Delta\kappa = \kappa_2 - \kappa_1$, $\langle\tilde{\mu}\rangle = (1-\theta_1)\mu_1 + \theta_1\mu_2$, and $\langle\tilde{\kappa}\rangle = (1-\theta_1)\kappa_1 + \theta_1\kappa_2$.

The explicit link relating the local stress in a locally layered composite to the macro stress modulation is analogous to Theorem 2.1 and is derived in Lipton and Stuebner (2006b). The physical significance of the macro stress

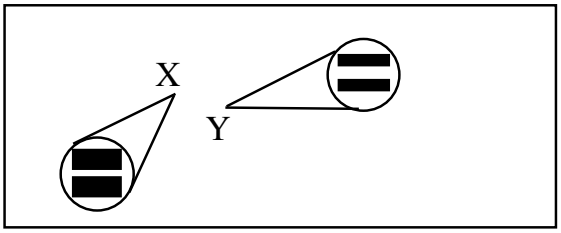

Fig. 8 The local layer thickness and oreintation can change across the cross section.

modulation function is that it provides an upper envelope on the local point wise stress amplitude inside material one when the layered microstructure is sufficiently fine, see Lipton and Stuebner (2006b).

The design variables for this problem are the local area fraction $\theta_1(\mathbf{x})$ of material one used in the layers and the layer orientation $\mathbf{n}(\mathbf{x})$. Here the layer orientation is written

$$\mathbf{n}(\mathbf{x}) = (\sin\gamma(\mathbf{x}), \cos\gamma(\mathbf{x}))$$

where $\gamma(\mathbf{x})$ is the local layer angle. As before $\theta_1(\mathbf{x})$ is free to change inside the design domain subject to the constraints given by (2.1), (2.2) and (2.3). Here the box constraints are given by $0 \leq \gamma < \pi$, $0.01 \leq \theta_1 \leq 0.99$, $\int_\Omega \theta_1 = 0.4 \times Area\, of\, \Omega$, $E_1 = 300Gpa$, $E_2 = 30Gpa$, and $\nu_1 = \nu_2 = 1/3$. We reiterate that the box constraints on θ_1 ensure that the design domain is completely filled with composite material.

The overall compliance of the structure is given by

$$C(\theta_1, \gamma) = \int \mathbf{g} \cdot \mathbf{u}^H \, ds, \tag{4.8}$$

where the integral is taken over the boundary of the design domain and $\mathbf{g}$ is the boundary traction field. The design problem for minimizing the overall compliance is given by

$$\min_{\theta_1\, \gamma} \{C(\theta_1, \gamma)\}, \quad \text{subject to constraints on } \theta_1. \tag{4.9}$$

This design problem is shown to be well posed in Lipton and Stuebner (2006b). The optimal area fraction distribution for this problem is denoted by $\hat{\theta}_1$ and is displayed in Figure 10. The level curves of the associated macro stress modulation function for material one are plotted in Figure 11.

For the second design problem we minimize the macro stress modulation function associated with the stiff material (material one) over the cross section. Here the function to be optimized is given by

$$M(\theta_1, \gamma) = \int (f_1(\theta_1, \sigma^H))^p \, d\mathbf{x}, \tag{4.10}$$

where the integral is taken over the design domain and $1 \leq p < \infty$. The design problem for minimizing the local stress inside material one is given by

$$\min_{\theta_1\, \gamma} \{M(\theta_1, \gamma)\}, \quad \text{subject to constraints on } \theta_1. \tag{4.11}$$

This design problem is shown to be well posed in Lipton and Stuebner (2006b). For this example we choose $p = 1$.

The optimal area fraction distribution for this problem is denoted by $\hat{\theta}_1$ and is displayed in Figure 12. The level curves of the associated macro stress modulation function are plotted in Figure 13. Comparison of Figures 11 and 13 show that the zones of high stress amplitude are dramatically reduced by the minimum stress design displayed in Figure 12. While the overall compliance for the minimum stress design is three times higher than the minimum compliance design, see Table 1.

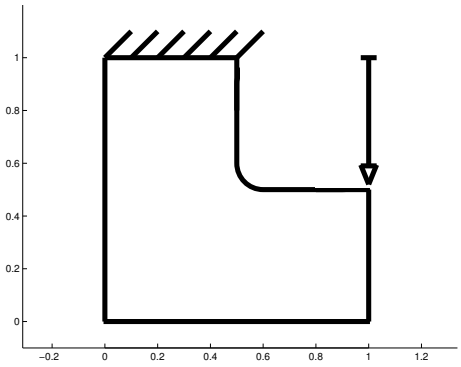

Fig. 9 Loading for the L-shaped domain for the plane strain problem.

Last the compliance minimization subject to a penalty on the pointwise stress inside material one is given by

$$\min_{\theta_1\, \gamma} \{C(\theta_1, \gamma) + \ell \times M(\theta_1, \gamma)\}, \quad \text{subject to constraints on } \theta_1. \tag{4.12}$$

where ℓ is the Lagrange multiplier for the stress constraint.

The optimal area fraction distribution for this problem is denoted by $\hat{\theta}_1$ and is displayed in Figure 14. The level curves of the associated macro stress modulation function are plotted in Figure 15. Comparison of Figures 11 and 15 show that the zones of high stress amplitude seen in the design for compliance minimization are dramatically reduced inside the design obtained from the stress penalized compliance minimization Figure 14. Table 1 shows that the overall compliance for the stress penalized design is twice as high as the compliance minimized design. It is interesting to note that the stress penalized design surrounds the regions of high stress amplitude with compliant material. This diminishes the effect of the stress concentrations arising from the abrupt change in boundary loading.

In each of these examples we relaxed the constraint (2.3) and all of the optimizations were carried out using square elements with bilinear shape functions for both

the elastic field variables and θ_1. The runs were carried carried out for a FEM mesh consisting of roughly 11,000 elements. The convergence histories for the minimum compliance design and minimum stress design are given in Figures 16 and 17.

The final two examples are carried out for the L-shaped design domain. This domain together with the boundary conditions and loading are shown in Figure 9. Here we compare the solutions to the minimum compliance design problem (4.9) with the minimum local stress design problem (4.11) posed on the L-shaped cross section. As seen in Figure 9, the L-shaped domain has a rounded reentrant corner that provides a stress concentration.

The design problems are carried out subject to the constraint that 40% of the cross-sectional area is occupied by material one. The optimal distribution of area fraction of material one $\hat{\theta}_1$ for the minimum compliance design problem (4.9) is displayed in Figure 18. The associated level curves of the macro stress modulation function for material one are plotted in Figure 19. The optimal distribution of area fraction of material one $\hat{\theta}_1$ for the minimum point wise stress design problem (4.11) is displayed in Figure 20 and the associated level curves of the macro stress modulation function for material one are plotted in Figure 21. Table 2 shows that the minimum compliance design has half the compliance as that of the minimum stress design. On the other hand comparison of Figures 19 and 21 show that the upper envelope for the point wise stress intensity as given by the level lines of the macro stress modulation function is significantly lower for the minimum stress design problem. Comparison of Figures 18 and 20 show that the minimum stress design problem removes the highest concentration of stiff material away from the reentrant corner. In these two examples we have relaxed the constraint (2.3) and all of the optimizations were carried out using triangular elements with linear shape functions for both the elastic field variables and θ_1. The runs were carried carried out for a FEM mesh consisting of roughly 72,000 elements. The convergence histories for the objective function for the minimum stress design is given in Figure 22.

References

Allaire G (2002) Shape Optimization by the Homogenization Method. Springer, New York.

Allaire G, Jouve F and Mallot H (2004) Topology optimization for minimum stress design with the homogenization method. Struct. Multidisc. Optim. Vol: 28 87–98.

Bendsøe M P and Sigmund O (2003) Topology Optimization, Theory, Methods and Applications. Springer, Berlin.

Cherkaev A and Kohn R V (1997) Topics in the Mathematical Modelling of Composite Materials. Progress in Nonlinear Differential Equations and their Applications. Birkhäuser, Boston.

Cherkaev A (2000) Variational Methods for Structural Optimization. Springer, New York.

Donoso A and Pedregal P (2005) Optimal design of 2D conducting graded materials by minimizing quadratic functionals in the field. Struct. Multidiscip. Optim. Vol: 30 360–367.

Duysinx P and Bendsøe M P (1998) Topology optimization of continuum structures with local stress constraints. Int. J. Num. Meths. Eng. Vol: 43 1453-1478.

Francfort G and Murat F (1987) Homogenization and optimal bounds in linear elasticity. Arch. Ration. Mech. Analysis Vol: 94 307 – 334.

Grabovsky Y (2001) Optimal design problems for two-phase conducting composites with weakly discontinuous objective functionals. Adv. in Appl. Math. Vol: 27 683–704.

Kohn R V and Strang G (1986) Optimal Design and Relaxation of Variational Problems. Communications on Pure and Applied Mathematics Vol: 34 Part I, 113-137, Part II, 139–182, Part III, 357-377.

Lewinski T and Telega J J (2000) Plates, Laminates and Shells. Asymptotic Analysis and Homogenization. World Scientific, Singapore.

Lipton R (2002) Relaxation through homogenization for optimal design problems with gradient constraints. J. Optim. Theory Appl. Vol: 114 27–53.

Lipton R (2002) Design of functionally graded composite structures in the presence of stress constraints. International Journal of Solids and Structures Vol: 39 2575–2586.

Lipton R (2004) Homogenization and design of functionally graded composites for stiffness and strength, in Nonlinear Homogenization and its Application to Composites, Polycrystals, and Smart Materials. Edited by P. Ponte Castaneda and J.J. Telega, NATO Science series II Mathematics, Physics, and Chemestry, Vol: 170, Springer Verlag, Berlin pp. 169–192.

Lipton R (2004) Stress constrained G closure and relaxation of structural design problems. Quarterly of Applied Mathematics Vol: 62 295–321.

Lipton R (2003) Assessment of the local stress state through macroscopic variables. Phil. Trans. R. Soc. Lond. A. Vol: 361 921–946.

Lipton R (2004) Homogenization theory and the assessment of extreme field values in composites with random microstructure. SIAM J. on Appl. Math. Vol: 65 475–493.

Lipton R and Stuebner M (2006a) Optimization of composite structures subject to local stress constraints. Computer Methods in Applied Mechanics and Engineering Vol: 196 66-75.

Lipton R and Stuebner M (2006b) Inverse homogenization and design of microstructure for pointwise stress control. Quarterly Journal of Mechanics and Applied Mathematics Vol: 59 131 – 161.

Lipton R and Velo A P (2002) Optimal design of gradient fields with applications to electrostatics. Nonlinear partial differential equations and their applications. Collge de France Seminar, Vol. XIV (Paris, 1997/1998). Stud. Math. Appl., Vol: 31, North-Holland, Amsterdam, pp. 509–532.

Love A (1944) A Treatise on the Mathematical Theory of Elasticity. Dover, New York.

Lurie K (1993) Applied Optimal Control Theory of Distributed Systems. Plenum Press, New York.

Olhoff N (1996) On optimum design of structures and materials. Meccanica Vol: 31 143–161.

Pedregal P (2004) Constrained quasiconvexification of the square of the gradient of the state in optimal design. Quart. Appl. Math. Vol: 62 459–470.

Stuebner M (2006) An Inverse Homogenization Design Method for Stress Control in Composites. Ph.D. Thesis, LSU.

Tartar L (1994) Remarks on optimal design problems. Calculus of Variations, Homogenization and Continuum Me-

chanics, Edited by G. Buttazzo, G. Bouchitte, and P. Suquet, World Scientific, Singapore pp. 279–296.
Tartar L (2000) An introduction to the homogenization method in optimal design. Springer Lecture Notes in Mathematics, Vol: 1740, Springer, Berlin pp. 45–156.
Velo A P (2000) Optimal Design of Gradient Fields and Currents. Ph.D. Thesis, WPI.

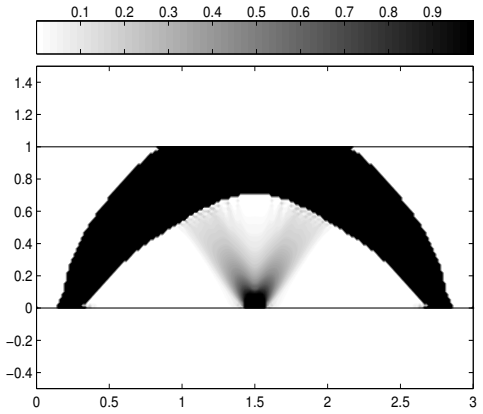

Fig. 10 Grey scale plot of $\hat{\theta}_1(\mathbf{x})$ for the minimum compliance design.

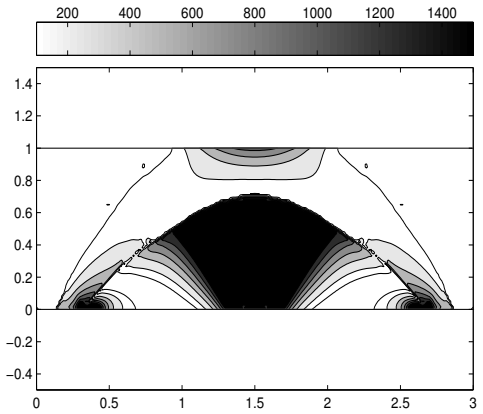

Fig. 11 Contour plot of $f_1(\hat{\theta}_1(\mathbf{x}), \sigma^H(\mathbf{x}))$ for the minimum compliance design.

Table 1 Technical data for the arch.

Optimized for:	phase 1	$C(\theta_1, \gamma)$	$M(\theta_1, \gamma)$
compliance	40.461%	1.876	1563.462
stress	40.122%	5.777	557.467
compliance and stress	40.364%	3.428	587.924

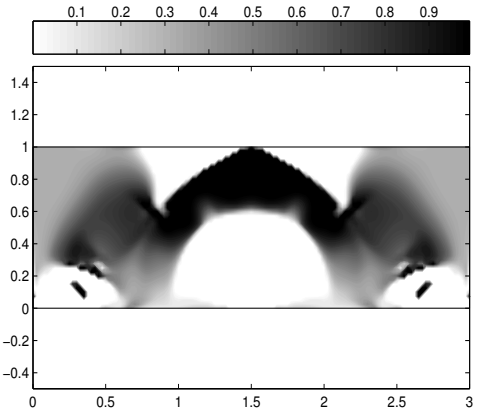

Fig. 12 Grey scale plot of $\hat{\theta}_1(\mathbf{x})$ for the minimum stress design.

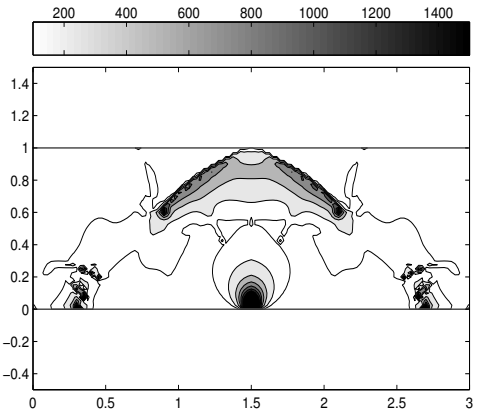

Fig. 13 Contour plot of $f_1(\hat{\theta}_1(\mathbf{x}), \sigma^H(\mathbf{x}))$ for the minimum stress design.

Table 2 Technical data for the L-shaped domain.

Optimized for:	phase 1	$C(\theta_1, \gamma)$	$M(\theta_1, \gamma)$
compliance	40.062%	6.525	7197.569
stress	39.793%	11.986	4737.866

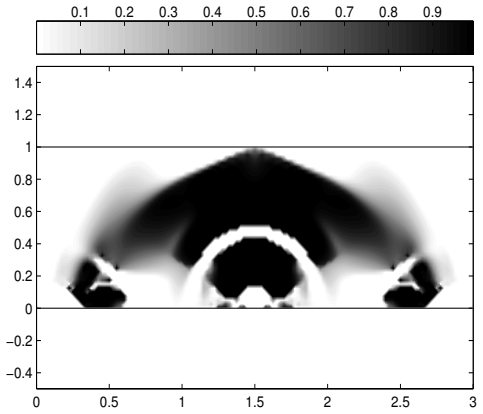

Fig. 14 Grey scale plot of $\hat{\theta}_1(\mathbf{x})$ for the stress penalized minimum compliance design.

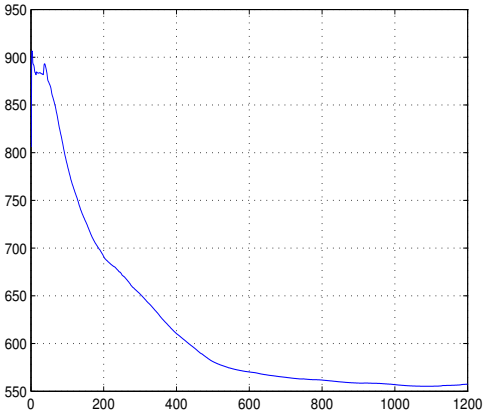

Fig. 17 Convergence history for $M(\theta_1, \gamma)$ for minimum stress design.

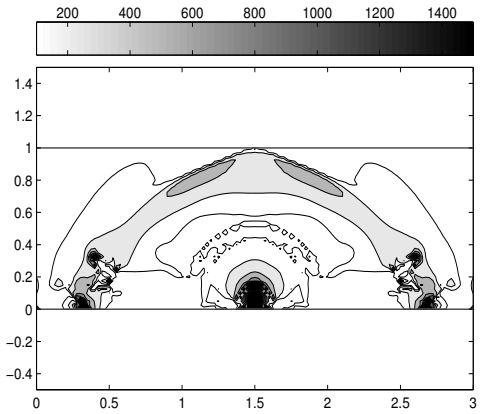

Fig. 15 Contour plot of $f_1(\hat{\theta}_1(\mathbf{x}), \sigma^H(\mathbf{x}))$ for the stress penalized minimum compliance design.

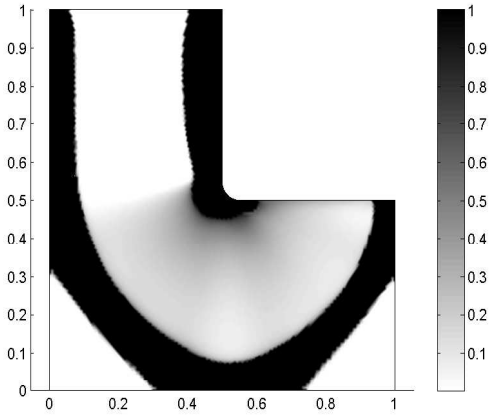

Fig. 18 Grey scale plot of $\hat{\theta}_1(\mathbf{x})$ for the minimum compliance design for the L-shaped domain.

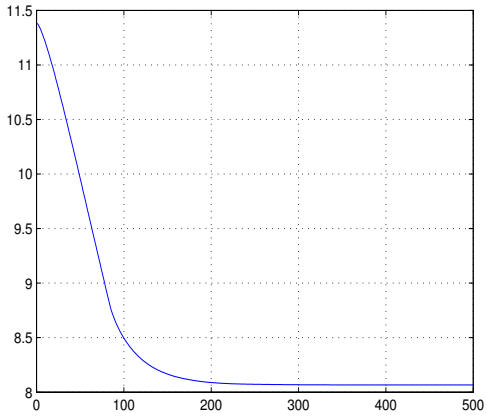

Fig. 16 Convergence history for $C(\theta_1, \gamma)$ for minimum compliance design.

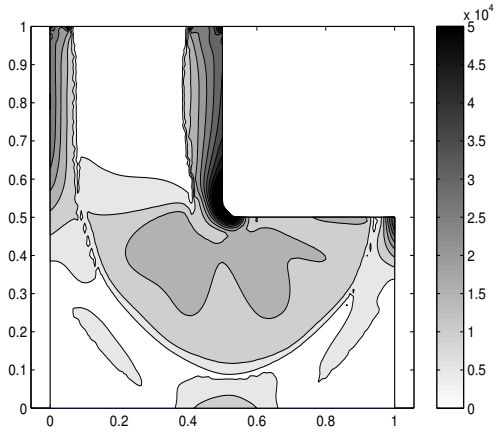

Fig. 19 Contour plot of $f_1(\hat{\theta}_1(\mathbf{x}), \sigma^H(\mathbf{x}))$ for the minimum compliance design for the L-shaped domain.

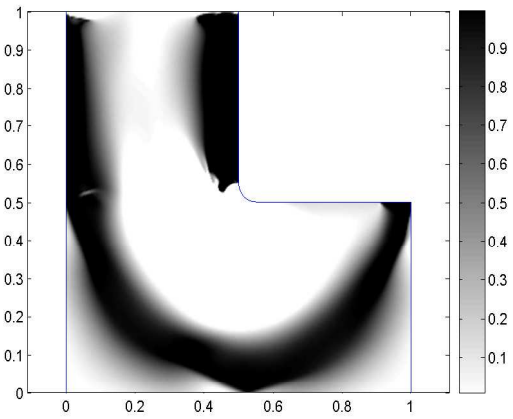

Fig. 20 Grey scale plot of $\hat{\theta}_1(\mathbf{x})$ for the minimum stress design for the L-shaped domain.

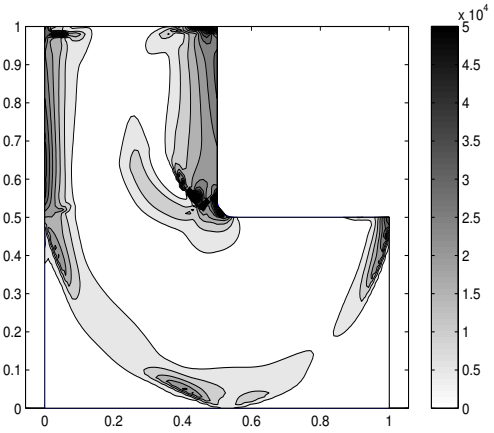

Fig. 21 Contour plot of $f_1(\hat{\theta}_1(\mathbf{x}), \sigma^H(\mathbf{x}))$ for the minimum stress design for the L-shaped domain.

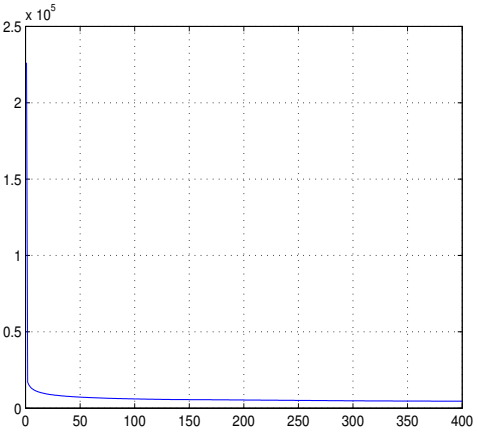

Fig. 22 The convergence history for $M(\theta_1, \gamma)$ for minimum stress design for the L-shaped domain.